CASE 3: Two-Dimensional Flow Control Analysis on the Hump Model

Sally A. Viken

Flow Physics and Control Branch, NASA Langley Research Center, Hampton, VA 23681-2199

Introduction

Computational analyses have been conducted on the Wall-mounted Glauert-Goldschmied type body ("hump" model) with the Full Unstructured Navier-Stokes 2-D (FUN2D) flow solver developed at NASA LaRC. This investigation uses the time-accurate Reynolds-averaged Navier-Stokes (RANS) approach to predict aerodynamic performance of the active flow control experimental database for the hump model. The workshop is designed to assess the current capabilities of different classes of turbulent flow solution methodologies, such as RANS, to predict flow fields induced by synthetic jets and separation control geometries. The hump model being studied is geometrically similar to that previously tested both experimentally and computationally at NASA LaRC [ref. 1 and 2, respectively].

Solution Methodology

The FUN2D flow solver is a node based, implicit, upwind flow solver used for computing flows around airfoil configurations discretized with an unstructured grid [ref. 3]. The governing equations (provided below) are the time-dependent RANS equations in conservation-law form, which are integrated in time to obtain a steady state solution. The inviscid fluxes are obtained on the faces of each control volume by using the flux-difference-splitting (FDS) technique of Roe [ref. 4]. A node-based algorithm is used in which the variables are stored at the vertices of the mesh and the equations are solved on non-overlapping control volumes surrounding each node. The viscous terms are evaluated with a finite-volume formulation that results in a central-difference-type scheme. The Spalart-Allmaras (SA) turbulence model is used in this investigation and all computations assume fully turbulent flow [ref. 5].

A two level iteration is used to achieve convergence of the discrete algebraic equations at each time-step. The outer iteration is a modified Newton method and employs a first-order Van Leer Jacobian (LHS) [ref. 6] driving the second-order residual vector (RHS). The inner iteration employs a red-black Gauss Siedel point-implicit algorithm to solve the equations at each step of the outer iteration. Twenty inner sub-iterations were used in all cases in this study. The SA turbulence model equations are weakly coupled to the hydrodynamic equation via the outer loop iteration.

For steady state computations, the solution is driven to convergence using an Euler implicit advancement in pseudo-time. For time-dependent computations, the solution is discretized in physical time with the second-order backwards differentiation formulae (BDF), while pseudo-time iterations are again employed to relax the equations [ref. 2, 7]. The linear system of equations resulting from either formulation is iteratively solved with a point-implicit procedure.

Governing Equations

The governing equations, the Reynolds-averaged Navier-Stokes equations, are written in conservative-law form to relate the rate of change of mass, momentum, and energy in a control volume of area A to the fluxes of these quantities through surface of the control volume. The non-dimensional equations presented in vector form are as follows:

$$\mathrm{A}\cdot\frac{\partial \mathbf{Q}}{\partial t} + \oint_{\partial\Omega} \vec{\mathbf{F}}_{\mathrm{i}}\cdot\hat{\mathbf{n}}\, dl - \oint_{\partial\Omega} \vec{\mathbf{F}}_{\mathrm{v}}\cdot\hat{\mathbf{n}}\, dl = 0$$

where $\hat{\mathbf{n}}$ is the outward-pointing unit normal to the surface of the control volume $\partial\Omega$. The solution vector **Q** containing the dependent variables is defined by

$$\mathbf{Q} = \begin{bmatrix} \rho \\ \rho u \\ \rho v \\ E \end{bmatrix}$$

The inviscid and viscous flux vectors through the surface of the control volume $\partial\Omega$, defined as $\vec{\mathbf{F}}_i$ and $\vec{\mathbf{F}}_{v,}$ respectively, are given by

$$\vec{\mathbf{F}}_i = \mathbf{f}\hat{i} + \mathbf{g}\hat{j} = \begin{bmatrix} \rho u \\ \rho u^2 + p \\ \rho uv \\ (E + p)u \end{bmatrix} \hat{i} + \begin{bmatrix} \rho v \\ \rho vu \\ \rho v^2 + p \\ (E + p)v \end{bmatrix} \hat{j}$$

$$\vec{\mathbf{F}}_v = \mathbf{f}_v\hat{i} + \mathbf{g}_v\hat{j} = \begin{bmatrix} 0 \\ \tau_{xx} \\ \tau_{xy} \\ u\tau_{xx} + v\tau_{xy} - q_x \end{bmatrix} \hat{i} + \begin{bmatrix} 0 \\ \tau_{yx} \\ \tau_{yy} \\ u\tau_{yx} + v\tau_{yy} - q_y \end{bmatrix} \hat{j}$$

The normal and shear stress terms and heat conduction terms are defined by

$$\tau_{xx} = (\mu + \mu_t) \frac{M_\infty}{Re} \frac{2}{3} [2u_x - v_y]$$

$$\tau_{yy} = (\mu + \mu_t) \frac{M_\infty}{Re} \frac{2}{3} [2v_y - u_x]$$

$$\tau_{xy} = (\mu + \mu_t) \frac{M_\infty}{Re} [u_y + v_x]$$

$$q_x = \frac{-M_\infty}{Re(\gamma - 1)} \left(\frac{\mu}{Pr} + \frac{\mu_t}{Pr_t} \right) \frac{\partial a^2}{\partial x}$$

$$q_y = \frac{-M_\infty}{Re(\gamma - 1)} \left(\frac{\mu}{Pr} + \frac{\mu_t}{Pr_t} \right) \frac{\partial a^2}{\partial y}$$

The equation of state for a perfect gas is used to define the pressure p

$$p = (\gamma - 1)\left[E - \rho \frac{(u^2 + v^2)}{2} \right]$$

and the laminar viscosity μ is determined through Sutherland's law

$$\frac{\mu}{\mu_\infty} = \frac{(1 + C^*)}{\left(\frac{T}{T_\infty} + C^*\right)} \left(\frac{T}{T_\infty}\right)^{\frac{3}{2}}$$

where C* = $\frac{198.6}{536.4}$ is Sutherland's constant divided by a free stream reference temperature which is defined to be 536.4° Rankine for Case Study #3.

The eddy viscosity, μ_t, is obtained by the turbulence closure model developed by Spalart and Allmaras [ref 5]. Again, the turbulent viscosity equation is solved separately from the flow equations at each time step, using the Euler implicit time-stepping scheme, resulting in a loosely coupled solution process.

Implementation and Case Specific Details

Unstructured Grids

Two-dimensional unstructured grids were generated for Case Study #3 analyses and provided at the website. The coordinates used for the unstructured grids were the 2-D non-dimensionalized theoretical model coordinates along with the tunnel geometry. These grids were generated with advancing front type point placement with iterative local re-meshing for grid quality improvement [ref. 8,9]. For the internal flow analyses conducted with the FUN2D code that will be presented at the workshop, the website unstructured Grid #1 and #2 were used. The forward extent of these grids is longer than the actual splitter plate length used in the wind tunnel experiment. These grids ran from –6.39c ahead of the leading edge of the model to 4.0c behind the leading edge of the model. This grid extent of -6.39c was chosen because it was found in preliminary CFD tests to yield a "run" long enough so that the computed boundary layer thickness *approximately* matched that of experimental data at x/c = -2.14 [figure 1]. The grid height is y/c = 0.90905, which corresponds with the actual height of 15.032 inches from the splitter plate to the ceiling of the tunnel test section. In addition, these grids were generated with the internal cavity modeled. The fine grid (website unstructured Grid #1) has 123703 nodes, 368476 faces, and 247404 cells. The minimum spacing at the viscous walls was set to be approximately 8.e-06. This minimum spacing yields a y+ value less than 1. The coarse grid (website unstructured Grid #2) has 57152 nodes, 169689 faces, and 114302 cells. The minimum spacing at the viscous walls was set to be approximately 1.6e-05. The upper grid boundary (test section ceiling) was set up to use inviscid-type grid spacing.

Initial calculations were conducted on the hump model using the grids described above for the baseline no-flow control condition. The experimental data for the baseline case showed a discontinuity in the Cp distribution at x/c = 0.48, which was not observed in the computational results. An unstructured grid was generated using the Quality Assurance (QA) coordinates provided at the website followed by further computational analyses. This grid has 122790 nodes, 365737 faces, and 245578 cells, with the minimum wall spacing yielding a y+ value less than 1. Computational results for the baseline no-flow condition analyzed with the QA coordinate grid and theoretical coordinate grid are compared with the experimental data [figure 2]. Computations with the QA grid show the sensitivity of the solution to the discontinuity in the hump model

surface geometry similar to that found experimentally. Outside of this localized discontinuity in the Cp distribution, the CFD solutions obtained with the QA coordinate grid and the theoretical coordinate grid compared well together. Grid studies were also conducted with the upper grid boundary defined to have viscous wall spacing, however only a slight increase in the flow acceleration over the hump model was achieved. All computations that will be presented at the workshop were run using the grids generated with the theoretical coordinates (unstructured Grids #1 and #2) that have inviscid-type grid spacing on the upper grid boundary.

Boundary Conditions

The boundary conditions on the hump model, the internal cavity walls, and the tunnel floor corresponded to no-slip between the fluid and the solid boundary at their interface, with a constant temperature wall that was set to the adiabatic wall temperature T_{aw}. The tunnel ceiling was treated as an inviscid surface. The internal "actuator" boundary at the bottom of the hump cavity was also treated as an inviscid surface for the baseline cases with no control. For the control cases, the "actuator" boundary condition corresponded to $\rho V(\xi, \eta = 0, t) = \text{Amplitude}*f(\xi)*\cos(\omega t)$ where $f(\xi) = 1$ (tophat distribution). The mass flux through the "actuator" boundary of the internal cavity was adjusted to obtain a peak velocity near 26.6 m/sec at the slot exit during the blowing part of the cycle [$(\rho V)_{max} = 0.001(\rho_{ref} a_{ref})$ was used to obtain this condition]. For inflow conditions, temperature was also specified on the "actuator" boundary from the experimental data. To obtain the boundary conditions at the tunnel inlet, the flow was assumed to be both inviscid and isentropic in this region so that quantities for the computation of the flux along the inflow boundary were obtained from two locally 1-D Riemann invariants. The Riemann invariants were considered constant along characteristics defined normal to the inflow boundary. At the downstream boundary, a back pressure of 0.99947 times reference pressure was specified in order to approximate the upstream conditions at the tunnel inlet.

Time-Step

The baseline and steady suction cases were run non-time-accurate, and achieved steady state convergence. The oscillatory suction/blowing case was run time-accurately using the second-order accurate Backward Differentiation Formulae (BDF) scheme. The assumption was made that the excitation frequency introduced at the "actuator" boundary was a perfect sine wave. The computational oscillatory cases were run time-accurately at least 20 shedding cycles to set up the flow field and then the Cp's were averaged over 20 cycles.

Test Conditions

Computational flow analyses were conducted on the hump model for $M_\infty = 0.1$, at Re = 936000. The two required test conditions for Case Study #3 were conducted along with the optional condition; the no-flow through the span slot, the suction case with suction rate of 0.01518 kg/sec through the slot, and the zero-net-mass-flux oscillatory suction/blowing case (frequency = 138.5 Hz, and peak velocity out of slot during blowing part of cycle = 26.6 m/s). Only two-dimensional computations were performed for these studies.

An example of the grid density effects are shown in figure 3, where the streamwise velocity profiles in the separated flow region at x/c = 0.8 for the suction case can be observed. The profiles for the fine and coarse level grids show that the grids are sufficiently resolved for the case analyzed.

REFERENCES

1. Seifert, A., and Pack, L. G., "Active Flow Separation Control on Wall-Mounted Hump at High Reynolds Numbers." AIAA Journal, Vol. 40, No. 7, July 2002.
2. Viken, S., Vatsa, V., and Rumsey, C., "Flow Control Analysis of the Hump Model with RANS Tools". AIAA 2003-0218, January 2003.

3. Anderson, W. K., and Bonhaus, D. L., "An Implicit Upwind Algorithm for Computing Turbulent Flows on Unstructured Grids," Computers & Fluids, Vol. 23, No. 1, 1994, pp. 1-21.
4. Roe, P., "Approximate Riemann Solvers, Parameter Vectors, and Difference Schemes," J. of Comp. Phys., Vol. 43, 1981, pp. 357-372.
5. Spalart, P.R. and Allmaras, S.R.,: "A One- Equation Turbulence Model for Aerodynamic Flows," AIAA 92-0439, January, 1992.
6. Van Leer, B., "Flux Vector Splitting for the Euler Equations," Lecture Notes in Physics, Vol. 170, 1982, pp. 501-502.
7. Carpenter, M. H., Viken, S. A., Nielsen, Eric J., "The Efficiency of High Order Temporal Schemes," AIAA Paper 2003-6334, January 2003.
8. Marcum, D. L., "Generation of Unstructured Grids for Viscous Flow Applications," AIAA Paper 95-0212, January 1995.
9. Marcum, D. L., and Weatherhill, N. P., "Unstructured Grid Generation Using Iterative Point Insertion and Local Reconnection," AIAA Journal, Vol. 33, No. 9, September 1995.

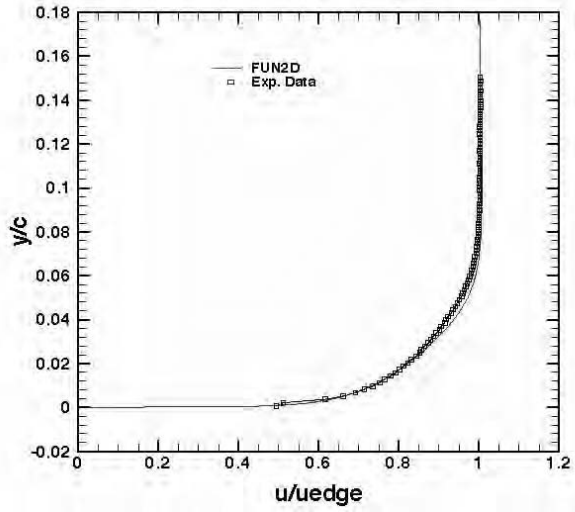

Figure 1. Velocity profile at x/c = -2.14 for baseline case (M_∞ = 0.1; Re = 936000).

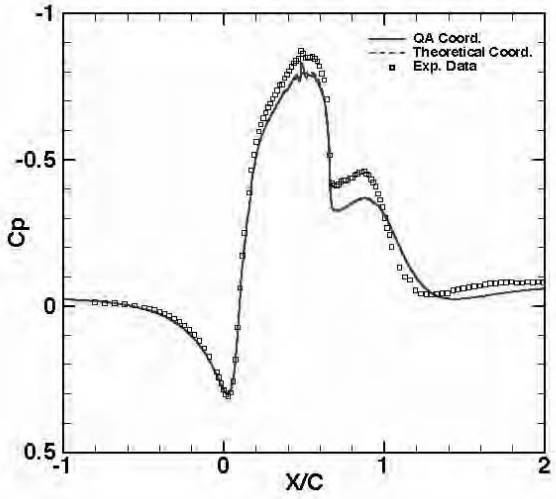

Figure 2. Baseline computational results versus experimental data (M_∞ = 0.1; Re = 936000).

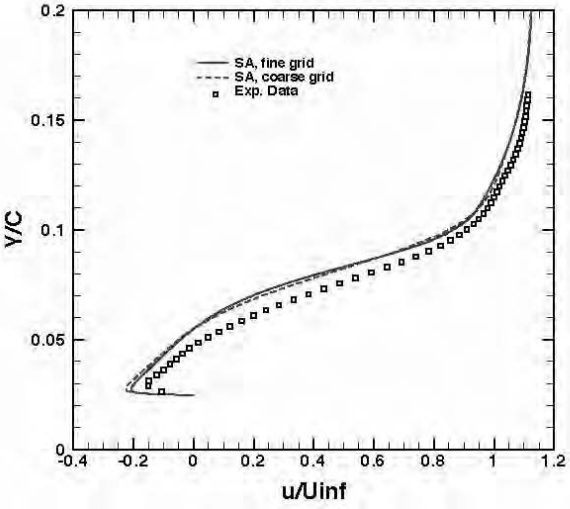

Figure 3. Velocity profiles at x/c = 0.8 for the suction case (M_∞ = 0.1; Re = 936000).